# Dual-mode of insulin action controls GLUT4 vesicle exocytosis

Yingke Xu,[1] Bradley R. Rubin,[1,2] Charisse M. Orme,[1,2] Alexander Karpikov,[3] Chenfei Yu,[2] Jonathan S. Bogan,[1,2] and Derek K. Toomre[1]

[1]Department of Cell Biology; [2]Section of Endocrinology and Metabolism, Department of Internal Medicine; and [3]Department of Diagnostic Radiology, Yale University School of Medicine, New Haven, CT 06520

Insulin stimulates translocation of GLUT4 storage vesicles (GSVs) to the surface of adipocytes, but precisely where insulin acts is controversial. Here we quantify the size, dynamics, and frequency of single vesicle exocytosis in 3T3-L1 adipocytes. We use a new GSV reporter, VAMP2-pHluorin, and bypass insulin signaling by disrupting the GLUT4-retention protein TUG. Remarkably, in unstimulated TUG-depleted cells, the exocytic rate is similar to that in insulin-stimulated control cells. In TUG-depleted cells, insulin triggers a transient, twofold burst of exocytosis. Surprisingly, insulin promotes fusion pore expansion, blocked by acute perturbation of phospholipase D, which reflects both properties intrinsic to the mobilized vesicles and a novel regulatory site at the fusion pore itself. Prolonged stimulation causes cargo to switch from ∼60 nm GSVs to larger exocytic vesicles characteristic of endosomes. Our results support a model whereby insulin promotes exocytic flux primarily by releasing an intracellular brake, but also by accelerating plasma membrane fusion and switching vesicle traffic between two distinct circuits.

## Introduction

In adipocytes and myocytes, insulin causes translocation of GLUT4 storage vesicles (GSVs) to the cell surface. Insertion of GLUT4 glucose transporters at the plasma membrane (PM) enhances glucose uptake and controls mammalian glucose homeostasis (Watson et al., 2004; Huang and Czech, 2007). Despite extensive study, where insulin acts to modulate GLUT4 trafficking is controversial (Dugani and Klip, 2005; Leney and Tavaré, 2009). One model posits that the main effect of insulin is to release GSVs from a deep, intracellular location (Bogan et al., 2003; Govers et al., 2004; Muretta et al., 2008). A second, more recent model challenges this view, and argues that fusion of vesicles at the PM is the major rate-controlling step (Huang et al., 2005; Koumanov et al., 2005; Bai et al., 2007).

Resolving where insulin acts has been hindered by several challenges. First, GLUT4 resides in several intracellular compartments, including the TGN, endosomes, and GSVs (Bryant et al., 2002). How GLUT4 traffics among these compartments is a matter of debate. Both "static retention" and "dynamic equilibrium" models have been proposed (Leney and Tavaré, 2009; Muretta and Mastick, 2009). A key difference is that in a "dynamic" model, insulin action at the PM can fully account for translocation. In contrast, the "static" model requires release from an internal, sequestered pool. Second, biochemical assays cannot easily quantify GLUT4 flux at individual trafficking steps, nor distinguish action on exocytic and endocytic pathways. Insulin may act at multiple sites, and increased PM fusion may actually result from release of an earlier rate-limiting step (Chen and Saltiel, 2007; Yu et al., 2007; Fujita et al., 2010). Finally, even with ultrasensitive imaging methods such as total internal reflection fluorescence microscopy (TIRFM), the small size of GSVs (∼60 nm) may preclude observation of unequivocal fusion events. Detection of larger, brighter endosomes may skew results. Indeed, using TIRFM, bona fide GLUT4-GFP

J.S. Bogan and D.K. Toomre contributed equally to this paper.

Correspondence to Derek K. Toomre: derek.toomre@yale.edu; or Jonathan S. Bogan: jonathan.bogan@yale.edu

Abbreviations used in this paper: FIPI, 5-fluoro-2-indolyl des-chlorohalopemide; FWHM, full-width at half-maximum; GSV, GLUT4 storage vesicle; PLD, phospholipase D; PM, plasma membrane; SDCM, spinning disc confocal microscopy; shRNA, short hairpin RNA; TfR, transferrin receptor; TIRFM, total internal reflection fluorescence microscopy.



The Rockefeller University Press $30.00
J. Cell Biol. Vol. 193 No. 4 643–653
www.jcb.org/cgi/doi/10.1083/jcb.201008135

full fusion events were rare or difficult to detect (Lizunov et al., 2005; Huang et al., 2007; Jiang et al., 2008).

To circumvent these issues, we used TUG knockdown to release retained vesicles and VAMP2-pHluorin as a new sensitive reporter for GSV fusion. Our data show that insulin switches traffic between two circuits and acts in a dual mode: the major activity is to release a brake, which retains GSVs intracellularly in unstimulated cells. A second activity is to accelerate fusion at the PM. Remarkably, insulin acts at the exocytic fusion pore, and promotes dilation of the pore and full vesicle fusion.

## Results and discussion

### Differentiation of 3T3-L1 cells induces a change in the size of GLUT4-containing exocytic vesicles

Single GLUT4 exocytic events in living cells may be caused by fusion of endosomes or GSVs at the PM. Distinguishing these vesicles is particularly important in 3T3-L1 adipocytes, which are heterogeneous and have significant GLUT4 in endosomes (Loo et al., 2009; Rubin and Bogan, 2009). We reasoned that endosomes and GSVs may have distinct TIRFM exocytic signatures (Fig. S1), as they differ considerably in size (~100–250 vs. ~50–70 nm diameters, respectively; Rodnick et al., 1992; Kandror et al., 1995). We found that GLUT4-GFP produced a bright vesicle fusion "flash" in 3T3-L1 preadipocytes, but fusion was difficult to detect in mature adipocytes (Fig. 1, A–D; Videos 1 and 2). This is consistent with the finding that GLUT4 traffics in endosomes in preadipocytes, but is targeted to GSVs in mature adipocytes (Shi and Kandror, 2005).

As a novel means to estimate a vesicle's size, we modeled how its intensity varies during docking ($I_d$) and fusion ($I_f$) in an exponentially decaying evanescent field (Fig. 1 E, black curve; see Materials and methods). The $I_d/I_f$ ratio is independent of the vesicle's absolute intensity and axial position, assuming that the fluorophore is uniformly distributed on the surface of a spherical vesicle. When docked, a larger vesicle will have a smaller fraction of fluorophores in the evanescent field, and $I_d/I_f$ will be smaller.

Our data show that GLUT4-containing exocytic vesicles had a diameter of 153 ± 42 nm in preadipocytes, which is consistent with GLUT4 recycling in endosomes, but that 56 ± 27 nm vesicles were the main exocytic carriers in mature adipocytes (Fig. 1 E). These smaller vesicles are identical in size to purified GSVs, measured using electron microscopy (Kandror et al., 1995). In addition, 92% of GLUT4 colocalized with transferrin receptor (TfR) in TIRFM images of preadipocytes, but only 57% colocalized in adipocytes (Fig. S2 A). These data support the finding that GSVs fuse directly with the PM.

### Validation of VAMP2-pHluorin as a new probe to visualize GSVs

To better identify GSV exocytosis, we used VAMP2-pHluorin. VAMP2 is an established component of GSVs (Ramm et al., 2000; Williams and Pessin, 2008; Bogan and Kandror, 2010), and pHluorin is a pH-sensitive fluorescent protein that becomes much more fluorescent when transferred from an acidic to a neutral environment (Miesenböck et al., 1998). We predicted that VAMP2-pHluorin would be a more sensitive reporter of GSV exocytosis compared with GLUT4-GFP.

Several criteria validated VAMP2-pHluorin as a probe to image GSVs. First, VAMP2-GFP colocalized extensively with GLUT4-DsRed (~74%; Fig. 2 A). Second, insulin increased the surface targeting of VAMP2-pHluorin (Fig. 2, B–D). Third, VAMP2-pHluorin and GLUT4-DsRed colocalized in fusing vesicles, as assessed using dual-color TIRFM (Fig. 2, E and F). Of note, kiss-and-run fusion events were observed using VAMP2-pHluorin, but not GLUT4-DsRed (Fig. 2 F). Finally, TUG disruption redistributed both GLUT4 (Yu et al., 2007) and VAMP2-pHluorin (Fig. S2, B–D) to the PM of unstimulated cells.

### Insulin regulates the stability of the fusion pore

The pH sensitivity of pHluorin ($pK_a$ = ~7.1), and even EGFP ($pK_a$ = ~6.0), has been exploited to visualize opening of the fusion pore, which causes a sudden rise in fluorescence (Barg et al., 2002; Bowser and Khakh, 2007). Using VAMP2-pHluorin, we confirmed that GSV fusion pore formation could be identified seconds before full vesicle collapse (Fig. 3, A and B; and Videos 3–5; Jiang et al., 2008). We define this operationally as a "transition time" (or fusion pore duration).

The transition time varied widely, from less than a second to several seconds (Fig. 3 B). Analysis of basal and insulin-stimulated full fusion events yielded probability distributions in Fig. 3 (C and D), with peaks at ~1 and ~3 s. A dual Gaussian fit showed that most (56%) events in basal cells were of longer duration; this fraction dropped to 22% in insulin-treated cells. Similar results were obtained using an arbitrary threshold (Figs. 3, C and D) or cumulative probability analysis (Fig. S3 A; P = 0.00035). Control experiments showed that insulin did not affect the transition time of VAMP2-pHluorin in preadipocytes (Fig. S3 B) or TfR-pHluorin in adipocytes (Fig. S3 C). Thus, insulin may act specifically on GSVs to accelerate the transition from pore formation to full expansion. Previous ~2–5 s "docking" times assigned using GLUT4-GFP (Huang et al., 2005; Bai et al., 2007) may be overestimated, as pore formation (a post-docking step) was not detected. In primary adipocytes, GLUT4 release was slow and constrained, prompting speculation that fusion pore opening may be regulated (Lizunov et al., 2005; Stenkula et al., 2010).

We wondered if a prolonged transition time in unstimulated cells might increase the frequency of kiss-and-run events, identified by a rapid fluorescence increase but no spread (Fig. 3 E; see Materials and methods). Strikingly, kiss-and-run events (defined operationally), in which the pore opened, closed, and the vesicle stayed in the region and slowly reacidified or moved axially, were common (~37%) in unstimulated cells, but were reduced to ~5% of events after insulin treatment (P < 0.01; Fig. 3 F). As chronic depletion of phospholipase D1 (PLD1) caused vesicles to "dock" at the PM, but not fuse (Huang et al., 2005), we tested if acute perturbation of PLD with a general antagonist (1-butanol)

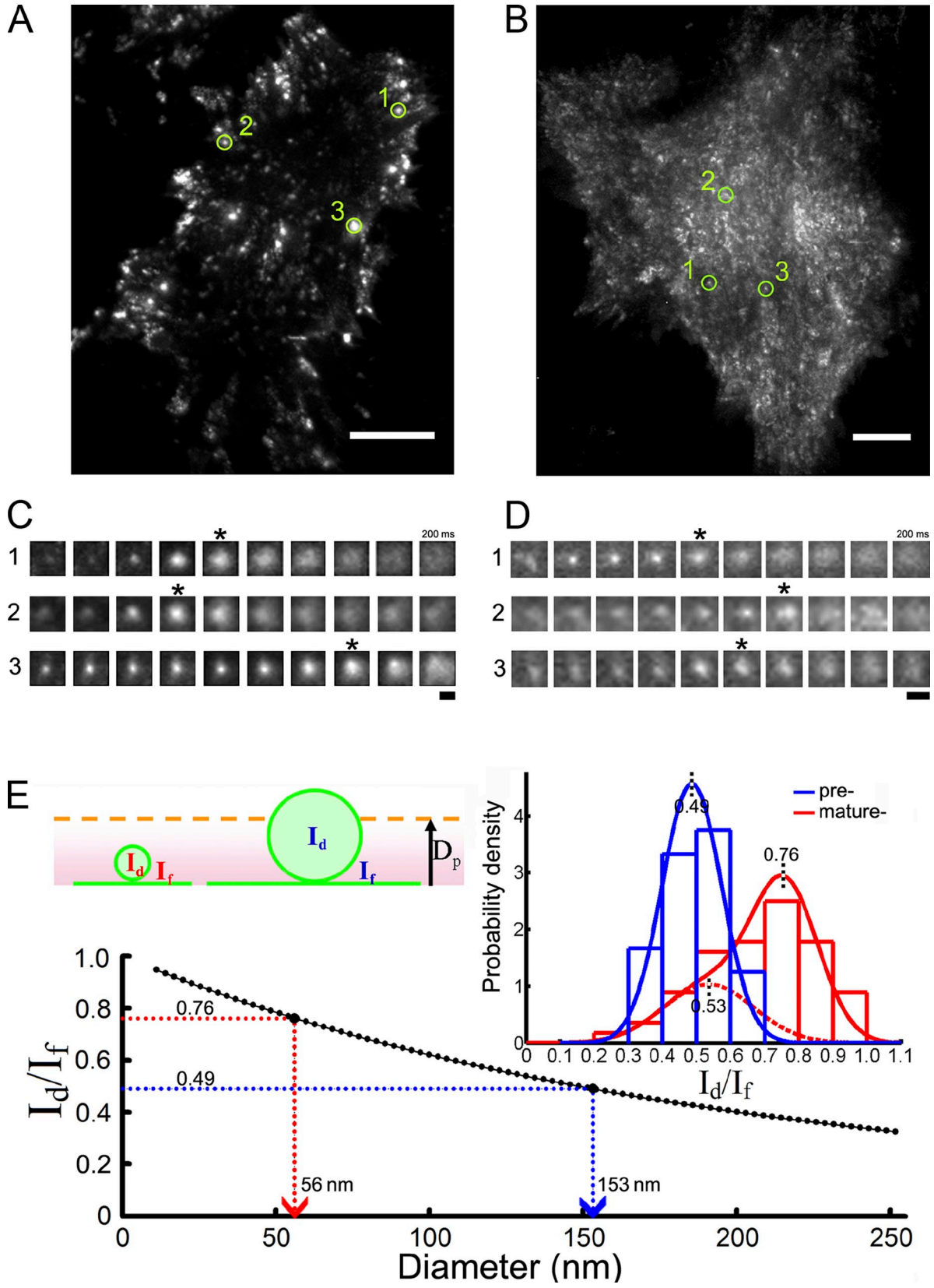


Figure 1. **3T3-L1 adipocyte differentiation induces a change in the size of GLUT4 vesicles.** (A–D) Single vesicle fusion events were visualized by TIRFM imaging of 3T3-L1 cells stably expressing GLUT4-GFP (see Videos 1 and 2). Maximum projection time-lapse (10 Hz) images of preadipocytes (A) and mature adipocytes (B) are shown, with galleries of single fusion events (asterisks) underneath (C and D). (E) Theoretical ratio of the fluorescence intensities of docked ($I_d$) to fully fused ($I_f$) membrane-labeled vesicles in an evanescent field of measured penetration depth, $D_p$ (98 nm), were modeled as a function of vesicle size (black curve, see Materials and methods). $I_d/I_f$ were measured for GLUT4 vesicles from preadipocytes and mature adipocytes and fitted to Gaussian distributions (inset), and the mean vesicle diameters were calculated using the black look-up curve (arrows). Bars: (A and B) 10 µm; (C and D) 1 µm.

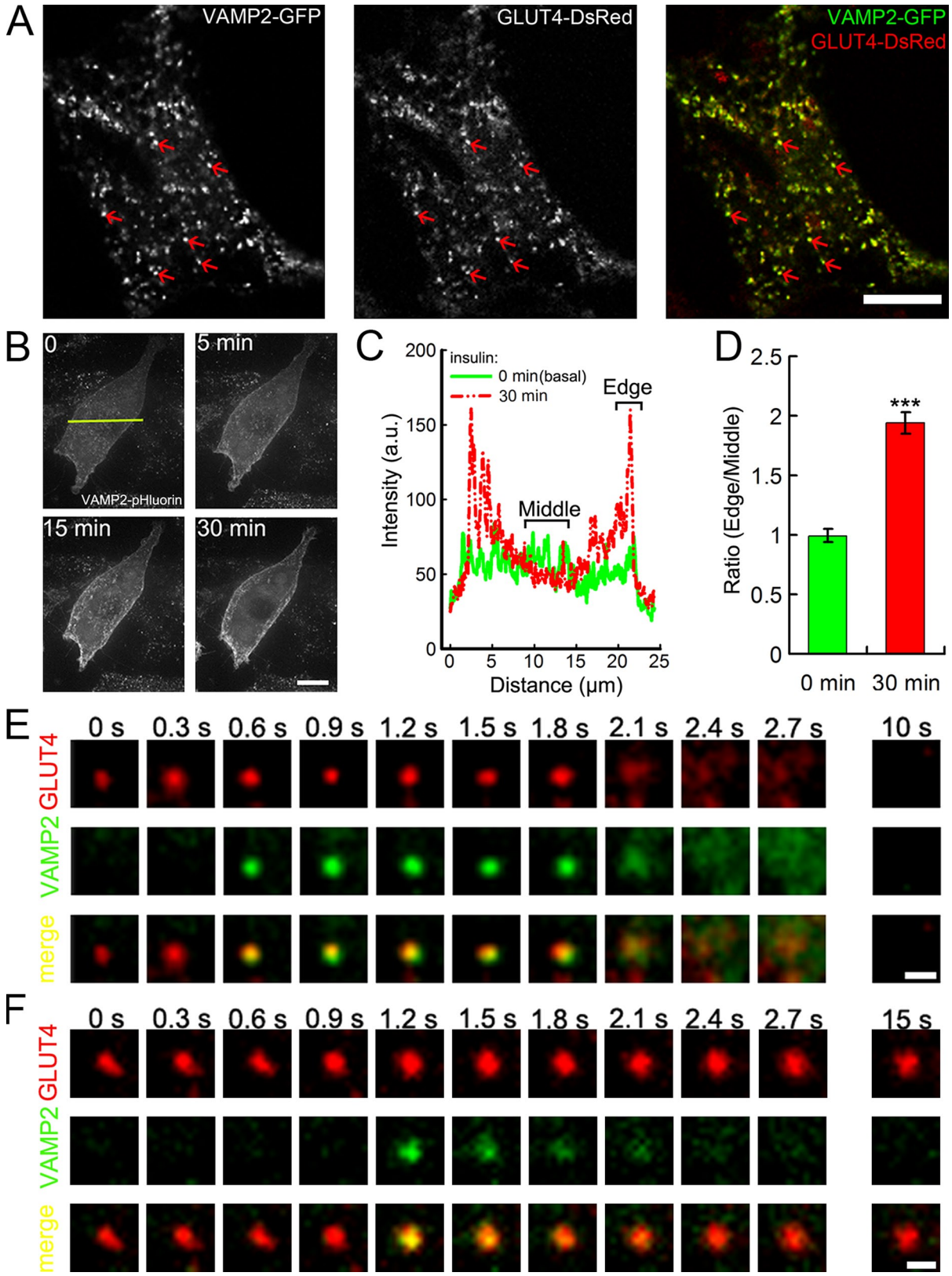


Figure 2. **Validation of VAMP2-pHluorin as a new probe to visualize GSVs.** 3T3-L1 adipocytes were electroporated with VAMP2 and/or GLUT4 and imaged by SDCM and TIRFM. (A) VAMP2-GFP and GLUT4-DsRed colocalize extensively (arrows). (B–D) Insulin-stimulated VAMP2-pHluorin translocation. 3T3-L1 adipocytes electroporated with VAMP2-pHluorin were imaged by 3D time-lapse SDCM. (B) Maximum z-projection images were taken before (0 min) and after (5–30 min) 100 nM insulin addition. (C) Fluorescence intensity line profiles (yellow line in B) were plotted for images before (green) and 30 min after (red) insulin. (D) The ratio of edge-to-middle intensities from line profiles of 10 cells was plotted (error bars indicate mean ± SEM; ***, $p < 0.001$). (E and F) VAMP2-pHluorin colocalizes with GLUT4-DsRed and allows detection of full fusion (E) and kiss-and-run (F) fusion events using dual-color TIRFM. Bars: (A and B) 10 μm; (E and F) 1 μm.

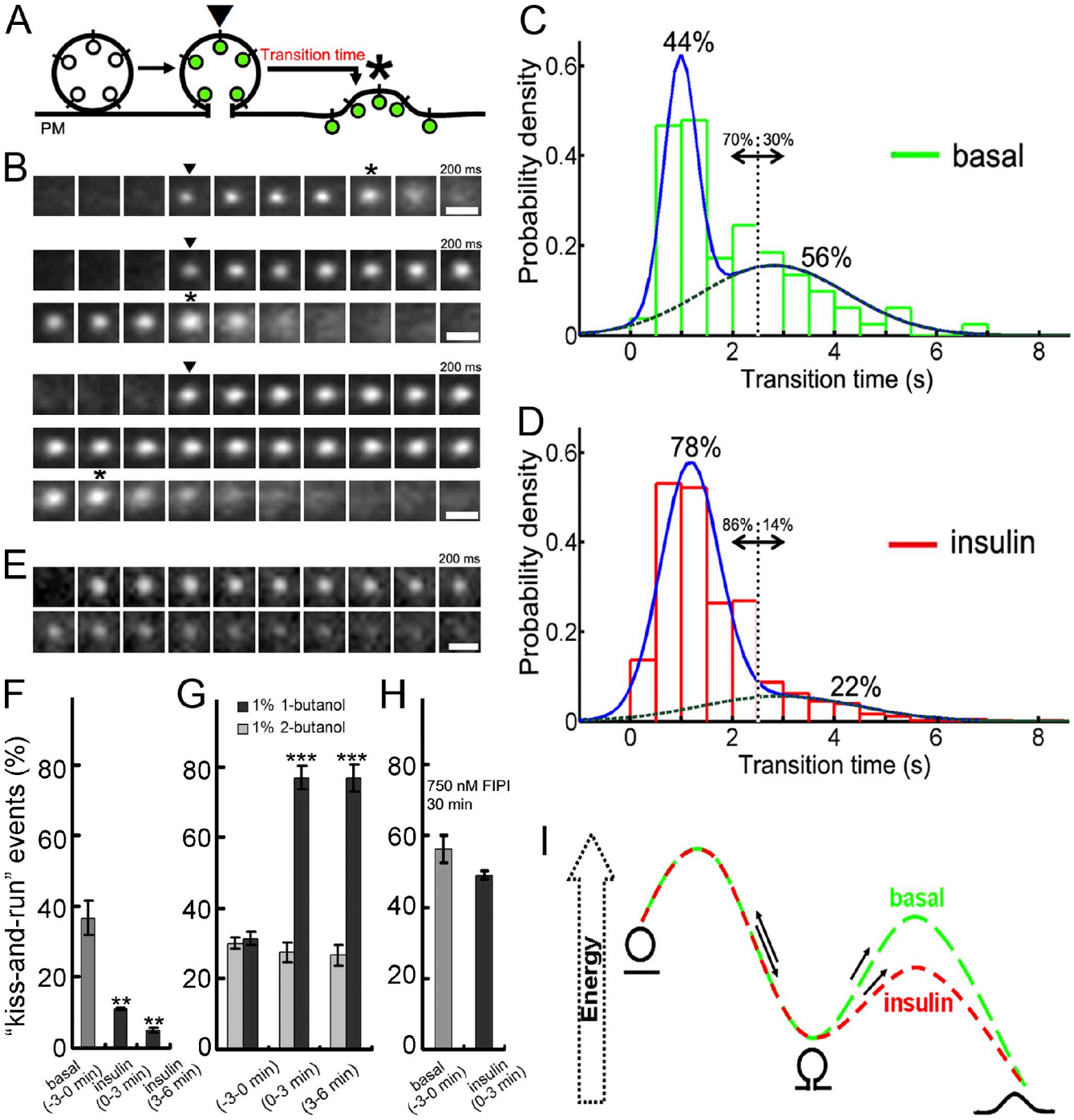


Figure 3. **Insulin regulates the stability of the vesicle fusion pore.** (A) pHluorin's fluorescence brightens (arrowhead) upon fusion pore formation, and then spreads laterally as the vesicle collapses into the PM (asterisk; see Fig. S1 [C and D] for fusion criteria). (B) Three examples of VAMP2-pHluorin fusion events with different durations of pore opening. (C and D) Vesicle "transition times" (arrowhead to asterisk) were measured in basal (C, *n* = 163) and insulin-stimulated (D, *n* = 894) cells, plotted as histograms, and fitted with a dual Gaussian distribution. (E) A representative kiss-and-run fusion event, whereby the signal slowly dimmed but did not spread (see Fig. S1 D). Bars, 1 µm. (F–H) Percentage of kiss-and-run events in basal and insulin-stimulated cells (F, *n* = 734 from three cells; **, P < 0.01), after addition of 1-butanol (G, *n* = 759 from three cells) or 2-butanol (*n* = 733 from three cells; ***, P < 0.001), and in FIPI-treated cells, before and after insulin (H, *n* = 150 from two cells). Error bars indicate mean ± SEM. (I) Working model of the energy landscape of vesicle fusion. Insulin reduces the barrier to full fusion after formation of the fusion pore.

or a new inhibitor (5-fluoro-2-indolyl des-chlorohalopemide [FIPI]; Su et al., 2009) affected the frequency of kiss-and-run events. Both drugs increased the frequency of kiss-and-run events in basal and insulin-stimulated cells (Figs. 3, G and H; 62 ± 5% for 1-butanol after insulin stimulation); as a control, 2-butanol had no effect (Fig. 3 G). These data implicate PLD in the regulation of fusion pore dynamics. Together, the data suggest a working model for GSV fusion (Fig. 3 I), whereby insulin lowers the barrier to full vesicle fusion and thus reduces the kiss-and-run frequency.

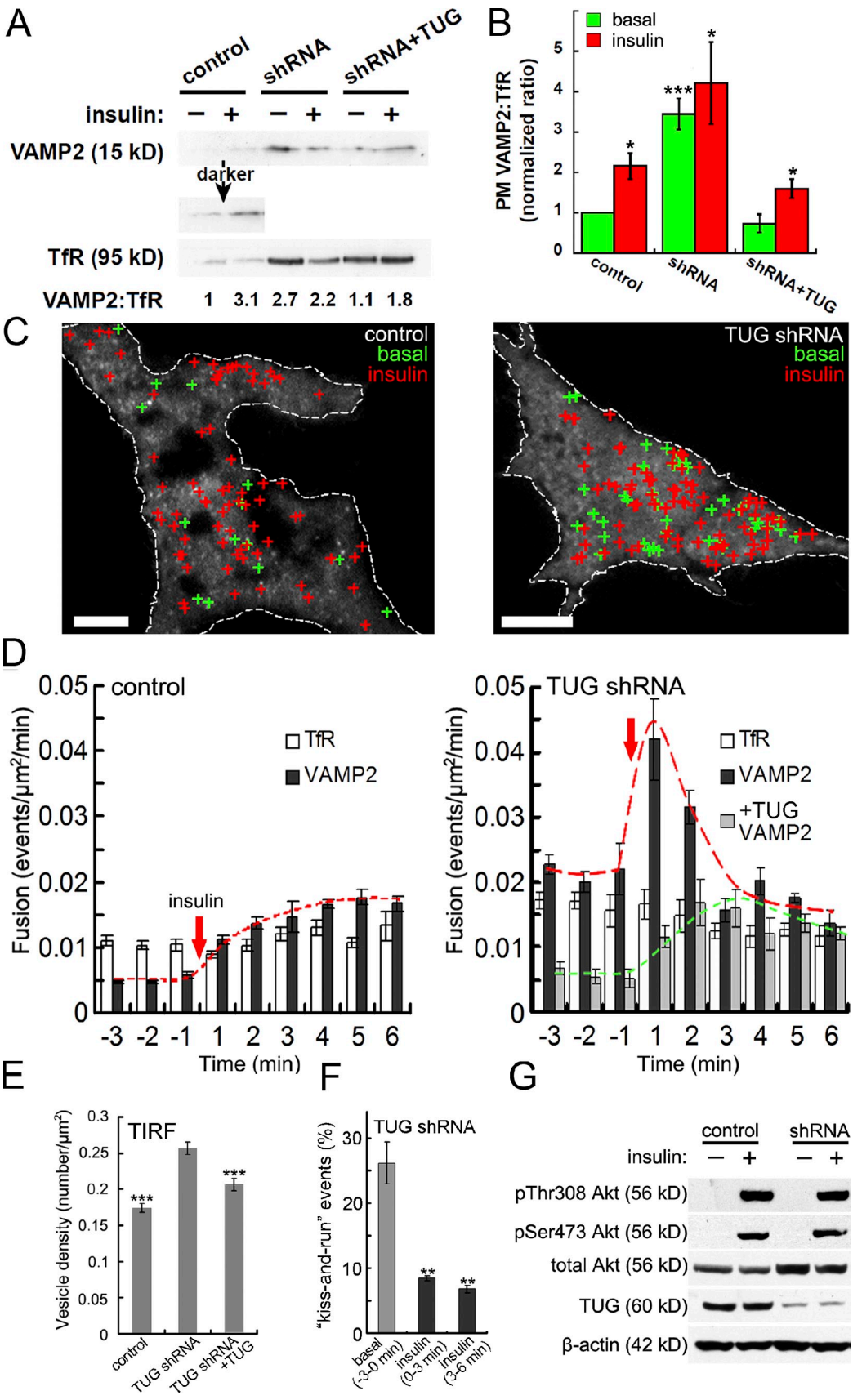


Figure 4. **TUG disruption increases GSV exocytic flux in unstimulated 3T3-L1 adipocytes.** (A) Immunoblots of PM fractions from control, TUG shRNA, and rescued (shRNA$^+$TUG) cells. The ratio of VAMP2 to TfR abundance is indicated for each sample, normalized to unstimulated control cells. (B) PM VAMP2:TfR was measured in three experiments by fractionation and immunoblotting. Mean ± SEM is plotted (error bars). *, $P < 0.05$; and ***, $P < 0.001$ relative to basal control. (C) VAMP2-pHluorin was expressed transiently in control and TUG shRNA cells, and fusion events (crosses) were marked over a 3-min window

### GSV translocation to the PM in the absence of TUG function

We next sought to bypass insulin signaling by manipulating TUG, a protein that retains GLUT4 intracellularly in unstimulated cells and that releases GLUT4 upon insulin stimulation (Bogan et al., 2003; Yu et al., 2007). We hypothesized that TUG disruption mobilizes GSV components (GLUT4 and VAMP2) to the PM. Supporting this idea, biochemical fractionation of 3T3-L1 adipocytes showed that VAMP2 was enriched in PM fractions from unstimulated cells containing a TUG short hairpin RNA (shRNA; Fig. 4, A and B). This effect was similar to that observed for GLUT4 (Yu et al., 2007). TfR distribution was unaffected, which is consistent with the idea that TUG regulates GSVs and not endosomes (Rubin and Bogan, 2009). Moreover, confocal microscopy revealed high PM targeting of VAMP2-pHluorin in unstimulated TUG shRNA cells (Figs. S2, B and D).

To test if TUG regulates GSV exocytosis, we imaged VAMP2-pHluorin in control and TUG shRNA adipocytes using TIRFM (Videos 3–5). Insulin greatly increased the exocytic rate in control cells, yet this rate was high before insulin addition in TUG shRNA cells (Fig. 4 C). Quantitative analysis (Fig. 4 D) revealed that insulin increased the VAMP2-pHluorin exocytosis rate by about fourfold in control 3T3-L1 adipocytes, similar to previous data (Huang et al., 2007; Lopez et al., 2009). As a control, the rate of TfR-pHluorin fusion was unchanged. Strikingly, in TUG shRNA cells, the basal rate of VAMP2-pHluorin exocytosis was similar to that in insulin-stimulated control cells (Fig. 4 D, broken red line), and was rescued by shRNA-resistant TUG (Fig. 4 D, broken green line). In the TUG shRNA cells, insulin promoted a transient (~1–2 min), twofold increase in the fusion rate. Accordingly, we tested if more vesicles are in close proximity (e.g., tethered) to the PM in these cells. We found that the density of GLUT4-GFP vesicles in the evanescent field in unstimulated TUG shRNA cells was increased 1.5-fold compared with control cells (Fig. 4 E; $P < 0.001$), and was rescued by shRNA-resistant TUG. These data support the idea that a TUG-regulated step is a major site at which insulin controls GSV exocytosis, and that insulin also stimulates GSV fusion with the PM.

We next tested if insulin decreased kiss-and-run events in TUG shRNA cells, which would support a direct action of insulin to regulate the fusion pore. In basal TUG shRNA cells, the kiss-and-run frequency was 26.2 ± 3.2%, and this rate decreased to 6.8 ± 0.6% (approximately fourfold) after insulin stimulation. The slightly lower basal rate was rescued by shRNA-resistant TUG (to 33.6 ± 2.4%). These data support a direct action of insulin on fusion pore dynamics. TUG knockdown cells had very short transition times ($t_{1/2}$ = ~0.5 s), which suggests an intrinsic property of the GSVs to promote fusion. Nonetheless, insulin slightly, but significantly ($P = 0.001$), shortened fusion pore duration (Fig. S3, D–F). Together, the data support the idea that in addition to mobilizing GSVs, insulin acts at the fusion pore itself.

As TUG depletion and insulin stimulation caused similar rates of exocytosis, we tested if insulin signaling is activated by TUG knockdown. Insulin-stimulated phosphorylation of Akt is proposed to be sufficient to induce GLUT4 translocation (Ng et al., 2008), yet data are equivocal on this point (Gonzalez and McGraw, 2006; Chang et al., 2007). TUG depletion did not cause Akt phosphorylation in unstimulated 3T3-L1 adipocytes, and insulin-stimulated Akt phosphorylation was similar in control and TUG shRNA cells (Fig. 4 G). Thus, the enhanced exocytic rate in basal TUG shRNA cells is independent of Akt.

### Small GSVs are mobilized by acute insulin stimulation

To analyze the size of insulin-stimulated exocytic vesicles, we extended our method based on the ratio of fluorescence intensities in docked and fused states. We reasoned that ratios of VAMP2-pHluorin intensities after fusion pore opening and after full fusion would permit us to assess vesicle size, and to resolve if insulin regulates distinct exocytic carriers. In basal adipocytes, vesicles containing VAMP2-pHluorin were the same size as those containing TfR-pHluorin, which supports the idea that they originate from endosomes (Fig. 5 A). After brief (3–6 min) insulin stimulation, small vesicles, identical in size to GLUT4-GFP vesicles in mature adipocytes, were the predominant exocytic carrier (Fig. 5, A and B). Similarly sized exocytic vesicles were observed in unstimulated TUG shRNA cells, which supports the idea that TUG regulates GSVs (Fig. 5 B). We hypothesized that GSV cargo might not engage the TUG retention mechanism during continued insulin exposure. Supporting this idea, only larger-sized vesicles fused at the surface of cells after prolonged insulin stimulation (Fig. 5, A and B), which is consistent with the idea that the GSV compartment is bypassed.

Intriguingly, the frequency of kiss-and-run events after prolonged (>15 min) insulin exposure was 25.5 ± 4.6% ($n = 230$ from two cells), much higher than the 5% observed after brief insulin stimulation. Thus, the effect of insulin to reduce kiss-and-run frequency at shorter time points (3–6 min) may in part be secondary to its mobilization of small vesicles. Yet, insulin markedly reduced the kiss-and-run frequency in TUG shRNA cells, as noted earlier, in which small vesicles are the predominant exocytic carrier. A parsimonious interpretation of these data is that GSVs have intrinsic properties that allow them to respond to an insulin signal at the fusion pore, which then specifically promotes full fusion of these vesicles.

### Dual-mode working model of insulin action

Our data indicate that GLUT4 traffics to the PM by two circuits, controlled by a dual brake/accelerator mode of insulin

before (green) and after (red) insulin stimulation (see Videos 3 and 4). Bars, 10 µm. (D) Frequencies of VAMP2-pHluorin and TfR-pHluorin fusion events in control ($n$ = 1,070 from five cells) and TUG shRNA 3T3-L1 adipocytes ($n$ = 895 from five cells). VAMP2-pHluorin events are also plotted for "rescued" TUG shRNA$^+$TUG cells (containing shRNA-resistant TUG, $n$ = 262 from three cells). Data are mean ± SEM (error bars). (E) GLUT4-GFP was transfected in control, TUG shRNA, and rescued (TUG shRNA$^+$TUG) cells and imaged by TIRFM. Density of single vesicles in the evanescent field of unstimulated cells ($n$ = 20 shRNA, 12 control, and 12 rescued cells; $D_p$ = 98 nm; $n$ = 10; ***, $P < 0.001$). (F) Percentage of kiss-and-run events in TUG shRNA cells ($n$ = 676 from three cells; **, $P < 0.01$). Error bars indicate mean ± SEM. (G) Immunoblots were performed as indicated on control and TUG shRNA adipocytes.

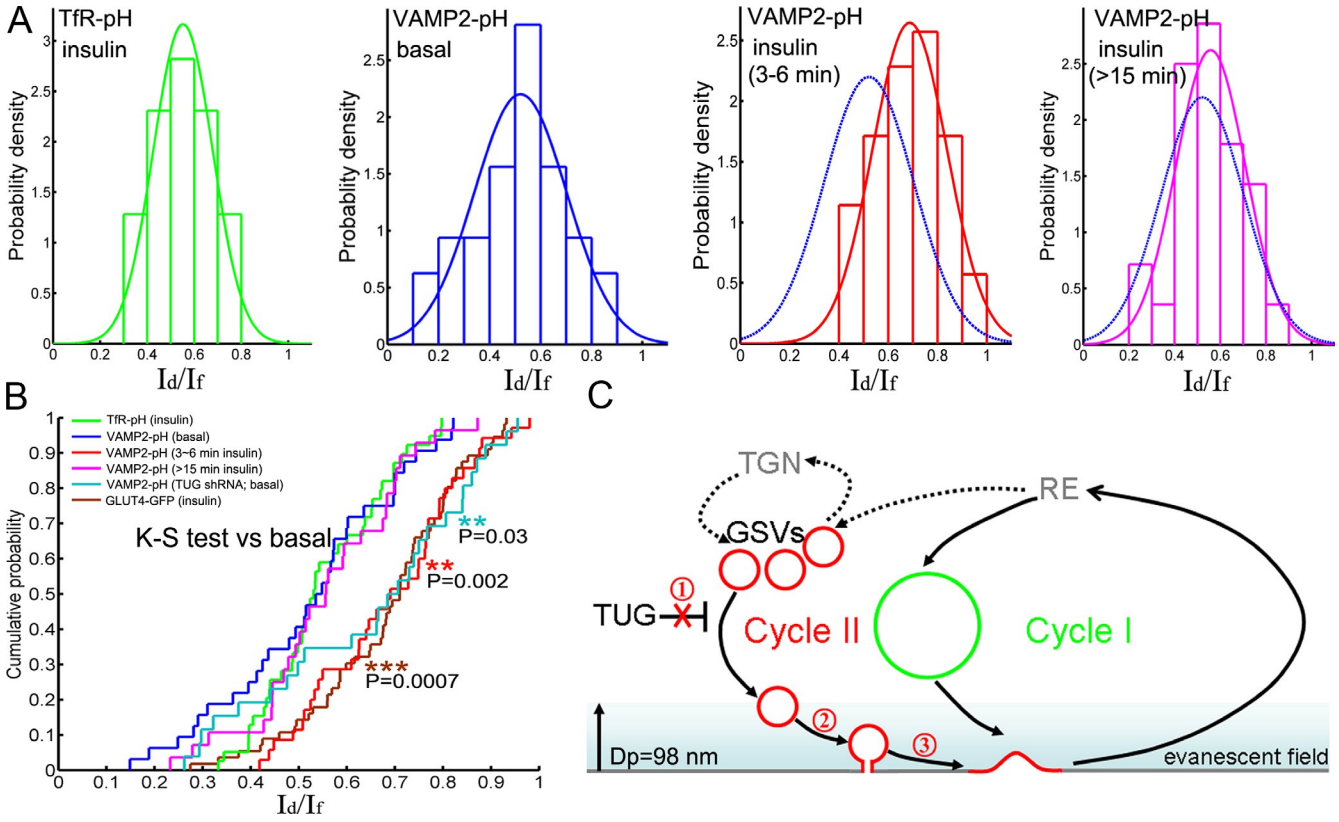


Figure 5. **Insulin regulates two distinct pools of GLUT4-containing vesicles.** 3T3-L1 adipocytes were transfected with plasmids encoding TfR-pHluorin or VAMP2-pHluorin, and imaged by TIRFM before and after 100 nM insulin stimulation. (A) Ratios of the fluorescence intensities of fusion pore open and fully fused states, $I_d/I_f$, were measured using the indicated reporters. Histograms were plotted and fitted with Gaussian distributions, with basal VAMP2-pHluorin is shown as a reference (blue). TfR-pHluorin data were similar for basal and insulin-stimulated cells; insulin data are shown. (B) Cumulative probability plots of data. Significance was assessed using a Kolmogorov-Smirnov test with basal VAMP2-pHluorin data as a reference set. (C) Dual brake–accelerator model of GSV translocation. Insulin acts both to release an intracellular brake (1) and to accelerate docking (2) and full fusion (3) at the PM, and switches vesicle traffic between two cycles (see text).

action (Fig. 5 C). First, insulin releases GLUT4 from TUG, which serves as a brake to prevent GSV translocation in unstimulated cells. Remarkably, the rate of GSV fusion was similar in unstimulated TUG knockdown cells and insulin-stimulated control cells. Thus, a major rate-limiting step for GSV translocation is upstream of vesicle fusion, which is counter to assertions based in part on cell-free assays (Koumanov et al., 2005; Leney and Tavaré, 2009) but consistent with a large immobile GLUT4 pool in basal adipocytes (Fujita et al., 2010). Second, insulin accelerates exocytosis of a fusion-ready pool of vesicles, as observed in TUG-depleted cells. This dual mode can account for the transition from basal to insulin-stimulated states.

Insulin also promoted a switch in the size of exocytic vesicles (Fig. 5). In preadipocytes and unstimulated adipocytes, the exocytic vesicles were identical in size to those containing TfR, whereas after acute (3–6 min) insulin stimulation, the predominant carriers were smaller (60 nm) vesicles (GSVs). The finding that GSV cargo is translocated in two distinct types of vesicles is not compatible with models in which insulin only increases the kinetics of exocytosis (Martin et al., 2006), but supports the idea that insulin enlarges the recycling pool (Govers et al., 2004; Muretta et al., 2008). Together with the result that larger vesicles are translocated during prolonged insulin exposure, our data unite the static retention and dynamic equilibrium models, as both participate in distinct phases of insulin action. How insulin switches cargo to the two circuits is unclear, but may involve AS160 modulation of Rab activity (Sakamoto and Holman, 2008).

Unexpectedly, insulin regulated fusion pore stability, reducing the fraction of kiss-and-run events by more than sevenfold and promoting full vesicle fusion. In part, this may reflect the mobilization of distinct carriers (GSVs) with increased propensity to fuse at the PM. Yet, the data also support an independent effect of insulin to regulate the fusion pore directly, likely through PLD. Thus, our data reveal the fusion pore as a novel site of insulin action, which may shed light on how insulin action is impaired in type 2 diabetes. In addition to PLD, Munc18c may mediate insulin effects at this site (Huang et al., 2005; Smithers et al., 2008). Finally, we speculate that fusion pore stability may be a control point in other regulated exocytic systems, such as neurons or pancreatic islets.

## Materials and methods

### Cell culture and biochemical methods

3T3-L1 cells were cultured in DME containing 10% fetal bovine serum, and differentiated in media supplemented with 500 µM isomethylbutylxanthine, 0.25 µM dexamethasone, and 160 nM insulin as described previously (Yu et al., 2007). After 8–10 d of differentiation, cells were electroporated

(Lonza) according to the manufacturer's instructions using Transfection solution "L" and cultured on glass-bottomed 35 mm dishes (MaTek Corporation) for microscopy (see Live cell imaging). Plasmids encoding superecliptic VAMP2-pHluorin, TfR-pHluorin, TfR-mCherry, and myc-GLUT4-DsRed were gifts of J. Rothman (Yale School of Medicine, New Haven, CT), C. Merrifield (Medical Research Council Laboratory of Molecular Biology, Cambridge, England, UK), M. Ehlers (Duke University Medical Center, Durham, NC), and M. Cormont (Centre Méditerranéen de Médecine Moléculaire, Nice, France), respectively. For stable expression of exogenous proteins or TUG shRNA, 3T3-L1 cells were infected with retroviruses as described previously (Bogan et al., 2001; Yu et al., 2007).

Subcellular fractionation and immunoblotting were performed as described previously (Yu et al., 2007). In brief, four to six 10-cm plates of adipocytes were used per condition. Cells were stimulated for 8–10 min using 480 nM insulin, washed in cold PBS, and scraped in ice-cold 250 mM sucrose, 10 mM Tris, pH 7.4, and 0.5 mM EDTA (TES) containing protease inhibitors (Complete; Roche). All subsequent steps were done at 4°C or on ice. Cells were homogenized in a Dounce-type Teflon tissue grinder (Kontes no. 22; VWR International), then centrifuged at 12,000 rpm for 15 min in an SS-34 rotor (Sorvall). The pellet was resuspended in TES and centrifuged again at 12,000 rpm for 20 min in an SS-34 rotor. To isolate PM fractions, the pellet was resuspended in ~1 ml TES, layered on top of a 1.12 M sucrose cushion (made in TES) in a ~2 ml centrifuge tube, and centrifuged at 36,000 rpm for 20 min in a TLS-55 rotor (Beckman Coulter). The interface was removed using a syringe, diluted in TES, and centrifuged at 37,000 rpm for 9 min in a TLA-120.2 rotor (Beckman Coulter). The pellet was resuspended and centrifuged again under identical conditions. The pellet was resuspended in SDS-PAGE sample buffer, and equal amounts of protein (by EZ-Q assays) in each sample were analyzed by SDS-PAGE and immunoblotting. NuPAGE gels and buffers were used (Invitrogen), and proteins were transferred to nitrocellulose membranes using a semidry apparatus. Detection was done both on film, using enhanced chemiluminescence (Thermo Fisher Scientific), and with an infrared imaging system (LI-COR Biosciences). For images acquired on film, densitometry was done on exposures in the linear range, which were digitized using a transilluminating flatbed scanner. Antibodies used were: mouse anti-myc (9E10; Covance), anti-Akt and phospho-Akt antibodies (Cell Signaling Technology), anti–β-actin (Abcam), anti-VAMP2 (a gift of J. Rothman), anti-TfR (a gift of P. De Camilli, Yale School of Medicine, New Haven, CT), and anti-TUG (Bogan et al., 2003). Antibodies were typically used at dilutions of 1:1,000. Secondary antibodies were conjugated to peroxidase (Bio-Rad Laboratories) for detection on film, or to IRDye700 or IRDye800 (LI-COR Biosciences) for digital imaging.

**Live cell imaging**

Electroporated 3T3-L1 adipocytes were imaged 15–20 h after transfection. Cells grown in MatTek chambers were serum starved for ~2 h, then imaged in KRH buffer, pH 7.4, containing 125 mM NaCl, 5 mM KCl, 1.3 mM $CaCl_2$, 1.2 mM $MgSO_4$, 20 mM D-glucose, 25 mM Hepes, and 0.2% bovine serum albumin. Insulin, FIPI, and 1- and 2-butanol were obtained from Sigma-Aldrich, and insulin was used at a final concentration of 100 nM. Cells were kept in an Air-therm (WPI) temperature-regulated environmental box at 37°C throughout the experiments.

The TIRFM setup was based on an IX-70 inverted microscope (Olympus), equipped with argon (488 nm) and argon/krypton (568 nm) laser lines (Melles Griot), a 60× 1.45 NA oil immersion objective lens (Plan-ApoN; Olympus), and a TIRFM condenser. Cells were imaged in one channel at 5–10 Hz or two channels by sequential excitation at 3–5 Hz, without binning, and detected with a back-illuminated Andor iXon887 EMCCD camera (512 × 512, 0.18 µm per pixel, 16 bits; Andor Technologies) with a 1.5× expansion lens. The TIRFM system was controlled by Andor iQ software, and the calculated depth of the evanescent field was 98 nm (see TIRFM calibration).

A Yokagawa-type spinning disc confocal microscope system was used for fast 4D imaging (PerkinElmer). The system was mounted onto an inverted microscope (IX-71; Olympus) quipped with a 1 Kb × 1 Kb EM charge-coupled device camera (Hamamatsu Photonics). The spinning disc confocal microscopy (SDCM) system was controlled by Volocity software, cells were imaged by using a 100× 1.4 NA oil objective lens, and exposure times were 0.1–0.25 s.

**TIRFM calibration**

Silica beads (Lot GK1529943W; Kisker-Biotech) with a 20-µm diameter were used for TIRFM calibration, as described previously (Mattheyses and Axelrod, 2006). The bead diameter was determined by taking a z-stack image using PIFOC piezo device (Physik Instrumente). The penetration depth (decay to 1/e or ~37%) of the evanescent field was calculated to be 98 nm for the TIRFM experiments.

**Vesicle size calculation**

To calculate the hypothetical size-dependent change in TIRFM fluorescence intensity caused by geometric collapse of a "docked" spherical vesicle in an exponentially decaying evanescent field (see Fig. 1 E), we performed a numerical simulation. Specifically, to calculate the theoretical change in fluorescence intensity from a docked ($I_d$) state (or fusion pore open state, Fig. 5) that contains a surface-labeled (2 nm shell) sphere of arbitrary radius, R (in nm), to a fused "pancake" state ($I_f$) of 4 nm thickness and radius $\sqrt{2}R$ (to mimic collapse into the cell PM), we computed the intensity in both states by numerical integration using the formula:

$$I = \iiint C(x,y,z)\exp(-z/d)dxdydz,$$

where C is unity inside of the "shell" or "pancake" and zero outside. The numerical integration was performed using MATLAB (MathWorks), using a penetration depth of 98 nm. Of note, this ratiometric calculation does not depend on the real distance of the PM to the glass surface and the intensity of the evanescent field $I_0$ at the glass surface.

**Image analysis**

Stacks of time-lapse images were processed and analyzed using algorithms implemented in ImageJ 1.42 (National Institutes of Health) and custom-written MATLAB programs. Images were prepared with Photoshop (Adobe); for display purposes, highly magnified images of single vesicles were "bicubic" smoothed. Videos were compressed with QuickTime Pro (Apple) using a JPEG 2000 algorithm. No nonlinear algorithms were used to alter fluorescent signals. Colocalizations were quantified using ImageJ and the "colocalization" plugin JACoP (provided by F. Cordelieres, Institut Curie, Orsay, France). The degree of overlap of markers within individual cells was determined using Pearson's correlation coefficient. Single vesicles in the TIRFM field were identified by ImageJ with the "particle detector" plugin (provided by I. F. Sbalzarini, Eidgenössische Technische Hochschule Zürich, Zürich, Switzerland).

For analysis of single fusion events, each acquired image sequence was manually reviewed multiple times to visually identify putative vesicle fusion events. The coordinates of the fusion events were marked and a small region of interest around each fusion was used for further analysis. Circular regions with diameters of 10 pixels (~1.8 µm) were used to calculate the intensity of single vesicles. The local background, the average intensity of a ring just outside this circle, was subtracted. The fusion profiles were analyzed with the implementation of a Gaussian fit. The integrated intensity, peak intensity and full-width at half-maximum (FWHM) of a Gaussian distribution were used to validate and distinguish between full fusion and kiss-and-run fusion events (Fig. S1, C and D). The peak intensity drops with a concurrent increase in FWHM when a vesicle undergoes full fusion (Fig. S1 C), whereas a kiss-and-run fusion event was defined operationally as having only a decrease in peak intensity without an increase of the FWHM (Fig. S1 D). For GLUT4-GFP fusion events, the intensity of docked vesicles, $I_d$, was monitored in the penultimate frames before full fusion events of intensity $I_f$. For VAMP2-pHluorin or TfR-pHluorin, $I_d$ was assigned to the mean intensity of a vesicle after the opening of the fusion pore, but before full fusion.

Binned counts of events were normalized such that bin areas summed to unity: each normalized bin height represents the probability per unit bin of observing the values in that bin. These observed probability densities were fitted with Gaussian probability densities using a maximum likelihood estimation in the Statistics Toolbox of MATLAB. In some cases, a mixture of two Gaussian probability densities was used:

$$\frac{\alpha}{\sigma_1\sqrt{2\pi}}e^{-x^2/2\sigma_1^2} + \frac{1-\alpha}{\sigma_2\sqrt{2\pi}}e^{-x^2/2\sigma_2^2},$$

whereby $\alpha$ is fractional contribution of the first Gaussian, and $\sigma_1$ and $\sigma_2$ are the standard deviations of the two Gaussians. Unless otherwise indicated, data are presented as the mean ± SEM, and were analyzed using a Student's *t* test.

**Online supplemental material**

Fig. S1 shows how single vesicle fusion events were analyzed, and includes examples of GLUT4-GFP in 3T3-L1 preadipocytes and mature adipocytes, and of VAMP2-pHluorin full fusion and kiss-and-run events in mature 3T3-L1 adipocytes. Fig. S2 shows that differentiation of 3T3-L1

adipocytes causes the targeting of GLUT4 to TfR-negative vesicles, as imaged by TIRFM. SDCM shows that VAMP2-pHluorin is distributed to the cell surface in both basal and insulin-stimulated TUG knockdown cells. Fig. S3 shows that insulin regulates VAMP2-pHluorin fusion pore dynamics in mature 3T3-L1 adipocytes, and reduces the transition time from pore opening to full vesicle fusion. Control experiments demonstrate that there is no effect of insulin on fusion pore dynamics in preadipocytes, or in mature adipocytes containing TfR-pHluorin. The effect of insulin is also observed in TUG shRNA cells. The supplemental videos present data that are summarized and quantified in the main text and figures. Video 1 shows TIRFM imaging of exocytosis of GLUT4-GFP in a 3T3-L1 preadipocyte. Video 2 presents TIRFM of GLUT4-GFP in a mature insulin-stimulated 3T3-L1 adipocyte. Video 3 shows TIRFM of VAMP2-pHluorin translocation in a wild-type 3T3-L1 adipocyte. Video 4 shows TIRFM of VAMP2-pHluorin in a TUG knockdown 3T3-L1 adipocyte. Video 5 shows a high-magnification cropped view of VAMP2-pHluorin exocytosis after insulin stimulation in a 3T3-L1 adipocyte. Online supplemental material is available at http://www.jcb.org/cgi/content/full/jcb.201008135/DC1.

We thank Drs. J. Rothman, P. De Camilli, C. Merrifield, M. Ehlers, M. Cormont, and E. Karatekin for reagents and advice.

This work was supported by fellowships to Y. Xu (China Postdoctoral Science Foundation 20080441255 and NSFC 30770596), B.R. Rubin (American Heart Association), and C.M. Orme (National Institutes of Health [NIH] F30DK086109), as well as by grants to J.S. Bogan (W. M. Keck Foundation and NIH R01DK075772) and D.K. Toomre (NIH DP2OD002980), and the Cell Biology Core of the Yale Diabetes Endocrinology Research Center (P30DK45735).

Submitted: 24 August 2010
Accepted: 11 April 2011

## References

Bai, L., Y. Wang, J. Fan, Y. Chen, W. Ji, A. Qu, P. Xu, D.E. James, and T. Xu. 2007. Dissecting multiple steps of GLUT4 trafficking and identifying the sites of insulin action. *Cell Metab.* 5:47–57. doi:10.1016/j.cmet.2006.11.013

Barg, S., C.S. Olofsson, J. Schriever-Abeln, A. Wendt, S. Gebre-Medhin, E. Renström, and P. Rorsman. 2002. Delay between fusion pore opening and peptide release from large dense-core vesicles in neuroendocrine cells. *Neuron*. 33:287–299. doi:10.1016/S0896-6273(02)00563-9

Bogan, J.S., and K.V. Kandror. 2010. Biogenesis and regulation of insulin-responsive vesicles containing GLUT4. *Curr. Opin. Cell Biol.* 22: 506–512. doi:10.1016/j.ceb.2010.03.012

Bogan, J.S., A.E. McKee, and H.F. Lodish. 2001. Insulin-responsive compartments containing GLUT4 in 3T3-L1 and CHO cells: regulation by amino acid concentrations. *Mol. Cell. Biol.* 21:4785–4806. doi:10.1128/MCB.21.14.4785-4806.2001

Bogan, J.S., N. Hendon, A.E. McKee, T.S. Tsao, and H.F. Lodish. 2003. Functional cloning of TUG as a regulator of GLUT4 glucose transporter trafficking. *Nature*. 425:727–733. doi:10.1038/nature01989

Bowser, D.N., and B.S. Khakh. 2007. Two forms of single-vesicle astrocyte exocytosis imaged with total internal reflection fluorescence microscopy. *Proc. Natl. Acad. Sci. USA*. 104:4212–4217. doi:10.1073/pnas.0607625104

Bryant, N.J., R. Govers, and D.E. James. 2002. Regulated transport of the glucose transporter GLUT4. *Nat. Rev. Mol. Cell Biol.* 3:267–277. doi:10.1038/nrm782

Chang, L., S.H. Chiang, and A.R. Saltiel. 2007. TC10alpha is required for insulin-stimulated glucose uptake in adipocytes. *Endocrinology*. 148:27–33. doi:10.1210/en.2006-1167

Chen, X.W., and A.R. Saltiel. 2007. TIRFing out studies on Glut4 trafficking. *Dev. Cell*. 12:4–5. doi:10.1016/j.devcel.2006.12.008

Dugani, C.B., and A. Klip. 2005. Glucose transporter 4: cycling, compartments and controversies. *EMBO Rep.* 6:1137–1142. doi:10.1038/sj.embor.7400584

Fujita, H., H. Hatakeyama, T.M. Watanabe, M. Sato, H. Higuchi, and M. Kanzaki. 2010. Identification of three distinct functional sites of insulin-mediated GLUT4 trafficking in adipocytes using quantitative single molecule imaging. *Mol. Biol. Cell*. 21:2721–2731. doi:10.1091/mbc.E10-01-0029

Gonzalez, E., and T.E. McGraw. 2006. Insulin signaling diverges into Akt-dependent and -independent signals to regulate the recruitment/docking and the fusion of GLUT4 vesicles to the plasma membrane. *Mol. Biol. Cell*. 17:4484–4493. doi:10.1091/mbc.E06-07-0585

Govers, R., A.C. Coster, and D.E. James. 2004. Insulin increases cell surface GLUT4 levels by dose dependently discharging GLUT4 into a cell surface recycling pathway. *Mol. Cell. Biol.* 24:6456–6466. doi:10.1128/MCB.24.14.6456-6466.2004

Huang, S., and M.P. Czech. 2007. The GLUT4 glucose transporter. *Cell Metab.* 5:237–252. doi:10.1016/j.cmet.2007.03.006

Huang, P., Y.M. Altshuller, J.C. Hou, J.E. Pessin, and M.A. Frohman. 2005. Insulin-stimulated plasma membrane fusion of Glut4 glucose transporter-containing vesicles is regulated by phospholipase D1. *Mol. Biol. Cell*. 16:2614–2623. doi:10.1091/mbc.E04-12-1124

Huang, S., L.M. Lifshitz, C. Jones, K.D. Bellve, C. Standley, S. Fonseca, S. Corvera, K.E. Fogarty, and M.P. Czech. 2007. Insulin stimulates membrane fusion and GLUT4 accumulation in clathrin coats on adipocyte plasma membranes. *Mol. Cell. Biol.* 27:3456–3469. doi:10.1128/MCB.01719-06

Jiang, L., J. Fan, L. Bai, Y. Wang, Y. Chen, L. Yang, L. Chen, and T. Xu. 2008. Direct quantification of fusion rate reveals a distal role for AS160 in insulin-stimulated fusion of GLUT4 storage vesicles. *J. Biol. Chem.* 283:8508–8516. doi:10.1074/jbc.M708688200

Kandror, K.V., L. Coderre, A.V. Pushkin, and P.F. Pilch. 1995. Comparison of glucose-transporter-containing vesicles from rat fat and muscle tissues: evidence for a unique endosomal compartment. *Biochem. J.* 307:383–390.

Koumanov, F., B. Jin, J. Yang, and G.D. Holman. 2005. Insulin signaling meets vesicle traffic of GLUT4 at a plasma-membrane-activated fusion step. *Cell Metab.* 2:179–189. doi:10.1016/j.cmet.2005.08.007

Leney, S.E., and J.M. Tavaré. 2009. The molecular basis of insulin-stimulated glucose uptake: signalling, trafficking and potential drug targets. *J. Endocrinol.* 203:1–18. doi:10.1677/JOE-09-0037

Lizunov, V.A., H. Matsumoto, J. Zimmerberg, S.W. Cushman, and V.A. Frolov. 2005. Insulin stimulates the halting, tethering, and fusion of mobile GLUT4 vesicles in rat adipose cells. *J. Cell Biol.* 169:481–489. doi:10.1083/jcb.200412069

Loo, L.H., H.J. Lin, D.K. Singh, K.M. Lyons, S.J. Altschuler, and L.F. Wu. 2009. Heterogeneity in the physiological states and pharmacological responses of differentiating 3T3-L1 preadipocytes. *J. Cell Biol.* 187:375–384. doi:10.1083/jcb.200904140

Lopez, J.A., J.G. Burchfield, D.H. Blair, K. Mele, Y. Ng, P. Vallotton, D.E. James, and W.E. Hughes. 2009. Identification of a distal GLUT4 trafficking event controlled by actin polymerization. *Mol. Biol. Cell*. 20:3918–3929. doi:10.1091/mbc.E09-03-0187

Martin, O.J., A. Lee, and T.E. McGraw. 2006. GLUT4 distribution between the plasma membrane and the intracellular compartments is maintained by an insulin-modulated bipartite dynamic mechanism. *J. Biol. Chem.* 281: 484–490. doi:10.1074/jbc.M505944200

Mattheyses, A.L., and D. Axelrod. 2006. Direct measurement of the evanescent field profile produced by objective-based total internal reflection fluorescence. *J. Biomed. Opt.* 11:014006. doi:10.1117/1.2161018

Miesenböck, G., D.A. De Angelis, and J.E. Rothman. 1998. Visualizing secretion and synaptic transmission with pH-sensitive green fluorescent proteins. *Nature*. 394:192–195. doi:10.1038/28190

Muretta, J.M., and C.C. Mastick. 2009. How insulin regulates glucose transport in adipocytes. *Vitam. Horm.* 80:245–286. doi:10.1016/S0083-6729(08)00610-9

Muretta, J.M., I. Romenskaia, and C.C. Mastick. 2008. Insulin releases Glut4 from static storage compartments into cycling endosomes and increases the rate constant for Glut4 exocytosis. *J. Biol. Chem.* 283:311–323. doi:10.1074/jbc.M705756200

Ng, Y., G. Ramm, J.A. Lopez, and D.E. James. 2008. Rapid activation of Akt2 is sufficient to stimulate GLUT4 translocation in 3T3-L1 adipocytes. *Cell Metab.* 7:348–356. doi:10.1016/j.cmet.2008.02.008

Ramm, G., J.W. Slot, D.E. James, and W. Stoorvogel. 2000. Insulin recruits GLUT4 from specialized VAMP2-carrying vesicles as well as from the dynamic endosomal/trans-Golgi network in rat adipocytes. *Mol. Biol. Cell*. 11:4079–4091.

Rodnick, K.J., J.W. Slot, D.R. Studelska, D.E. Hanpeter, L.J. Robinson, H.J. Geuze, and D.E. James. 1992. Immunocytochemical and biochemical studies of GLUT4 in rat skeletal muscle. *J. Biol. Chem.* 267:6278–6285.

Rubin, B.R., and J.S. Bogan. 2009. Intracellular retention and insulin-stimulated mobilization of GLUT4 glucose transporters. *Vitam. Horm.* 80:155–192. doi:10.1016/S0083-6729(08)00607-9

Sakamoto, K., and G.D. Holman. 2008. Emerging role for AS160/TBC1D4 and TBC1D1 in the regulation of GLUT4 traffic. *Am. J. Physiol. Endocrinol. Metab.* 295:E29–E37. doi:10.1152/ajpendo.90331.2008

Shi, J., and K.V. Kandror. 2005. Sortilin is essential and sufficient for the formation of Glut4 storage vesicles in 3T3-L1 adipocytes. *Dev. Cell*. 9:99–108. doi:10.1016/j.devcel.2005.04.004

Smithers, N.P., C.P. Hodgkinson, M. Cuttle, and G.J. Sale. 2008. Insulin-triggered repositioning of munc18c on syntaxin-4 in GLUT4 signalling. *Biochem. J.* 410:255–260. doi:10.1042/BJ20070802

Stenkula, K.G., V.A. Lizunov, S.W. Cushman, and J. Zimmerberg. 2010. Insulin controls the spatial distribution of GLUT4 on the cell surface through

regulation of its postfusion dispersal. *Cell Metab.* 12:250–259. doi:10.1016/j.cmet.2010.08.005

Su, W., O. Yeku, S. Olepu, A. Genna, J.S. Park, H. Ren, G. Du, M.H. Gelb, A.J. Morris, and M.A. Frohman. 2009. 5-Fluoro-2-indolyl des-chlorohalopemide (FIPI), a phospholipase D pharmacological inhibitor that alters cell spreading and inhibits chemotaxis. *Mol. Pharmacol.* 75:437–446. doi:10.1124/mol.108.053298

Watson, R.T., M. Kanzaki, and J.E. Pessin. 2004. Regulated membrane trafficking of the insulin-responsive glucose transporter 4 in adipocytes. *Endocr. Rev.* 25:177–204. doi:10.1210/er.2003-0011

Williams, D., and J.E. Pessin. 2008. Mapping of R-SNARE function at distinct intracellular GLUT4 trafficking steps in adipocytes. *J. Cell Biol.* 180:375–387. doi:10.1083/jcb.200709108

Yu, C., J. Cresswell, M.G. Löffler, and J.S. Bogan. 2007. The glucose transporter 4-regulating protein TUG is essential for highly insulin-responsive glucose uptake in 3T3-L1 adipocytes. *J. Biol. Chem.* 282:7710–7722. doi:10.1074/jbc.M610824200